AIAA 80-0201R

Blade Loading and Spanwise Effects on Wake Characteristics of Compressor Rotor Blade

B. Reynolds* and B. Lakshminarayana†
The Pennsylvania State University, University Park, Pa.

An experimental investigation of the blade loading and spanwise effects on the rotor wake is presented. The investigation was limited to a study of a low subsonic and incompressible wake flow found downstream of a lightly loaded rotor. Measurements were made with a triaxial hot wire probe mounted in the stationary frame of reference at six radial and nine axial positions. At each measurement location, the rotor was run at different operating conditions to discern the effects of blade loading on the wake. Near- and far-wake measurements are given, including mean velocity and turbulence intensity characteristics. The loading and spanwise effects on rotor-wake characteristics were found to be substantial.

Nomenclature

c = chord length
C_D = section drag coefficient (based on mean velocity)
C_L = section lift coefficient (based on mean velocity)
L_{LS}, L_{TS} = wake width at half the depth on the leading and trailing surface sides of the wake, respectively
Q = resultant velocity in the relative (rotating) frame of reference
R = radius ratio $= r/r_t$
r, θ, z = radial, tangential, and axial coordinates, respectively ($z = 0$ at trailing edge)
S = blade spacing
s, n, r = streamwise, normal, and radial coordinates ($s = 0$ at trailing edge, $n = 0$ at the wake center)
s_o = streamwise virtual origin
U, V, W = radial, tangential, and axial velocities (mean) in rotating coordinate system
U_n, U_r, U_s = relative mean velocities in the normal, radial, and streamwise directions, respectively
u = radial mean velocity in the wake
u_n', u_r', u_s', = fluctuating components of relative velocities in the normal, radial, and streamwise directions, respectively
u', v', w' = fluctuating component of radial, tangential, and axial velocities
v, w = defect in relative tangential and axial mean velocities, respectively
Y = tangential distance from the wake centerline nondimensionalized by semiblade spacing $= 2r\theta/S$ ($\theta = 0$ at wake centerline, and Y is negative on the suction side and positive on the pressure side of the wake)
Z = axial distance from rotor blade trailing-edge nondimensionalized by chord length of rotor blade
δ = wake width $= 2(L_{LS} + L_{TS})$
θ^* = momentum thickness in wake
ρ = density
$\tau_r, \tau_z, \tau_\theta$ = normalized turbulence intensities in the radial, axial, and tangential directions, respectively $= (\overline{u'^2})^{1/2}/W_o$, $(\overline{w'^2})^{1/2}/W_o$, and $(\overline{v'^2})^{1/2}/W_o$
τ_s, τ_n, τ_r = normalized streamwise, normal, and radial intensities, respectively $= (\overline{u_s'^2})^{1/2}/U_{s_o}$, $(\overline{u_n'^2})^{1/2}/U_{s_o}$, and $(\overline{u_r'^2})^{1/2}/U_{s_o}$
i = incidence

Subscripts

c = at the wake centerline
d = defect in wake velocity
e = wake edge
m = maximum value in wake
o = in freestream
t = at the tip
$1, 2$ = inlet and outlet to rotor, respectively

Introduction

THE complex, three-dimensional compressor or fan rotor wake has significant effect on turbomachinery aerodynamic and acoustic characteristics and is of scientific interest, since it provides information on the effects of rotation and curvature on the development and decay of turbulent shear flows. Since the extent of the wake influences on turbomachinery performance is substantial, a better understanding of the flow is important for establishing improved design criteria, for predicting noise levels, and for determining flow induced vibrations. With the wake representing a dissipation of energy as it mixes with the freestream, studies of the rotor wake are essential for building quieter and more efficient turbomachinery.

The objective of the present research was to experimentally investigate the three-dimensional near- and far-wake characteristics of a compressor rotor. The research included a study of wake profiles and their decay characteristics, effects of varying blade loading, and the effects of spanwise position on the wake. The present investigation was limited to a study of a low subsonic and incompressible wake flow found downstream of a lightly loaded rotor. Systematic measurements of the wake at a variety of spanwise locations provided information as to the extent of three-dimensionality in the flow. At each spanwise location, measurements were made with the rotor set at different operating conditions to discern the effects of blade loading on the wake. Experimental measurements of the three-dimensional mean velocity and turbulence wake structure were made using a triaxial hot wire probe located in the stationary frame of reference behind the rotor.

Presented as Paper 80-0201 at the AIAA 18th Aerospace Sciences Meeting, Pasadena, Calif., Jan. 14-16, 1980; submitted April 17, 1980; revision received May 8, 1981.

*Graduate Assistant, presently Development Engineer, Avco Lycoming Division. Member AIAA.

†Professor of Aerospace Engineering and Director of Computational Fluids Dynamics Studies. Associate Fellow AIAA.

Experimental Facility and Program

Measurements reported in the present investigation were made using the Axial Flow Research Fan Facility at the Applied Research Laboratory of The Pennsylvania State University. A detailed description of the facility is given in Refs. 1 and 2. A 12-bladed (uncambered) rotor with the following specifications was installed: S/c (midspan) = 0.680, tip diameter = 0.54 m, hub-to-tip ratio = 0.44, blade chord = 15.2 cm, and stagger angle (midspan) = 45.0 deg. The rotor was operated at midspan blade incidences of 5, 10, and 15 deg.

Near- and far-wake measurements were made with a triaxial hot wire probe located downstream of the rotor in the stationary frame of reference. Five radial and a variety of axial measurement stations were selected to define the near- and far-rotor-wake characteristics at various spanwise locations. Blade loading was varied at each station to discern this effect on the rotor wake. A full description of this experimental program is presented in Ref. 2. The data processing procedure provided three-dimensional components of mean velocity, turbulence intensity, and Reynolds stresses across the wake.

Experimental Results: Interpretation and Correlation

The stationary triaxial probe measurements have been used to study the near- and far-wake characteristics downstream of the rotor, including spanwise and blade loading effects. Data are presented showing typical profiles of mean velocity and turbulence intensity. The variations of overall wake characteristics (such as wake centerline defect) with spanwise position are also given. A correlation is examined for total velocity defect at all of the blade loadings and spanwise positions tested. Velocity defect is defined as the difference between freestream and local mean velocities in the wake. Reynolds stress measurements are not presented in this paper.

Mean Velocity Profiles

All mean velocity data presented in this section are nondimensionalized by freestream axial velocities. Rotor relative tangential mean velocity data showed similar features to those found for the axial component and are not shown in this paper for the sake of brevity.

Axial Velocity

Axial mean velocity profiles of rotor wake are shown for $R = 0.721$ in Fig. 1. Similar results were obtained at other radial locations. The observed asymmetry in the wake profile is expected since the rotor blade suction surface boundary layer is thicker than the pressure surface boundary layer. The inviscid effect, larger freestream velocities on the suction side than on the pressure side, is also evident. However, the asymmetry is no more pronounced near the hub or end walls than at midspan. As a result of wake spreading and mixing with the freestream, approximate symmetry is found far downstream ($Z > 1.0$) at all spanwise measurement stations.

The rotor wake is shown to be thicker with larger defects at all spanwise positions for increased blade loadings (increased rotor blade incidence). Wake width is found to be larger at the spanwise stations away from midradius, representing significant hub- and end-wall effects on the structure of the rotor wake. For $Z > 1.0$, the rotor wake is found to have decayed to near the freestream value. The rotor-wake decay takes place through an exchange of momentum and energy from the freestream to the wake region and from one radius to another (through radial flows, which will be discussed later).

Radial Velocity

Variation of radial mean velocity across the rotor wake at $R = 0.721$ is illustrated in Fig. 2. Again, similar results were obtained at other radial locations. A radially outward

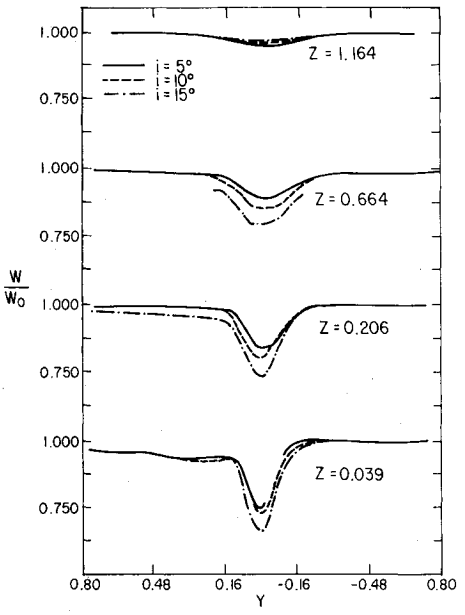

Fig. 1 Axial velocity profile at $R = 0.721$.

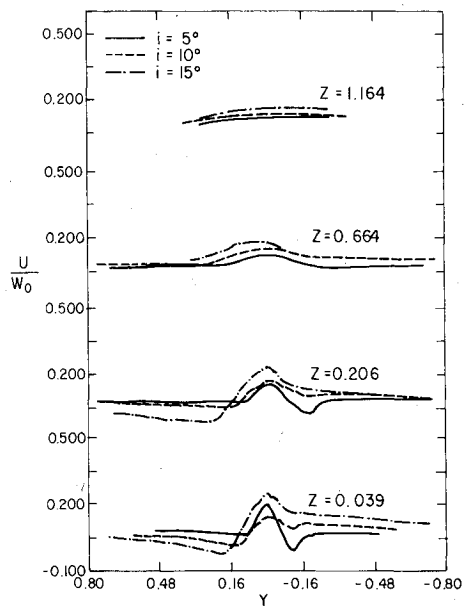

Fig. 2 Radial velocity profile at $R = 0.721$.

migration of flow is found in the rotor wake at all spanwise stations. The inviscid effect was also seen at all spanwise positions in the near-wake region with larger outward freestream radial velocities measured on the suction side of the wake than on the pressure side. While the maximum radial velocity difference across the wake was larger at $R = 0.907$, the large outward radial flows near the wake centerline are not found. This characteristic is a result of strong end-wall effects at this spanwise position. The radial flows in the wake and the inviscid effect have decayed substantially in the far-wake region ($Z > 1.0$)

Increased rotor blade incidence shows larger radial flows in the wake at all spanwise positions. As expected, larger loading also results in a significantly increased inviscid effect across the blade passage. The blade loading effects are still evident in the far-wake region for all of the spanwise stations measured. This exhibits the strong effect that past history of the flow has on the wake structure and decay.

Turbulent Intensity Profiles

Turbulence intensity measurements given in this section are nondimensionalized by freestream axial mean velocity. Tangential turbulence intensities are not shown for the sake of brevity since they showed similar characteristics as those shown by the axial intensity component.

Axial-Turbulence Intensity

Axial-turbulence intensity profiles at $R=0.907$ are shown in Fig. 3. The profiles were found to be highly asymmetric for all spanwise stations in the near wake. As expected from the development of the pressure and suction surface boundary layers, the turbulence intensities in the near wake are larger on the suction side of the wake centerline than on the pressure side. The axial turbulence intensity profiles in the far-wake region for $Z>1.0$ become symmetric at all spanwise measurement stations.

Larger axial-turbulence intensities are found at all spanwise stations for increased blade loadings (increased rotor blade incidence). This characteristic is still clearly discernible for all of the data shown in the far-wake region.

Axial-turbulence intensities in the wake at $R=0.907$ extend over a larger extent of the blade passage than at $R=0.721$ (midspan). The wake width of axial turbulence intensities is largest at $R=0.907$. These spanwise characteristics of the wake indicate that high levels of turbulent flow unsteadiness can be expected on a downstream stator at positions away from midradius.

Radial-Turbulence Intensity

The radial-turbulence intensity profiles are shown in Fig. 4 for the spanwise position of $R=0.721$. Similar to the axial component, radial-turbulence intensities exhibit a high degree of asymmetry at all spanwise measurement stations in the near wake. The level of radial-turbulence intensities is slightly less than the corresponding axial-turbulence intensities. However, the presence of a high radial component of turbulence intensity indicates the extent of three-dimensionality in the rotor-wake flow.

Increased blade loadings are found to result in increased radial-turbulence intensities in the wake at all spanwise positions. The blade loading effects are still evident at the far downstream stations ($Z>1.0$). At spanwsie positions away from midradius the blade loading effects on the radial turbulence intensities in the wake are stronger. This characteristic indicates the extent to which the hub- and end-wall flows affect the wake turbulence intensities.

As with axial-turbulence intensities, the radial-turbulence intensities in the near-wake extend over a larger portion of the blade passage at stations away from midradius.[2] This represents radially nonuniform three-dimensional turbulent unsteadiness that will be sensed by a downstream stationary blade row.

Variation of Wake Centerline Velocity or Defect Downstream

Decay of axial and tangential mean velocity defects at the wake centerline and maximum radial velocity difference in the wake are given in Figs. 5, 6, and 7, for $R=0.535$, 0.721, and 0.907, respectively. Data are shown in both the near- and far-wake regions at rotor blade incidence of 5, 10, and 15 deg.

The effects of varying blade loading are clearly seen for all three spanwise stations. As found in the profile data, larger axial and tangential defects and radial velocities in the wake are shown for increased blade loadings. This characteristic is discernible in both the near- and far-wake regions and is not found to be more pronounced at the measurement stations away from midradius. For this case, hub- and end-wall flow effects on the rotor wake did not increase with increasing blade loadings.

All three spanwise measurement stations indicate a rapid decay of the wake near the rotor blade trailing edge, consistent with the midspan results of Ref. 1. However, axial and

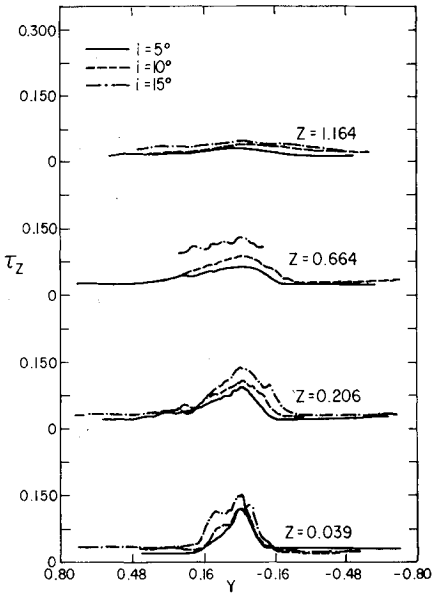

Fig. 3 Axial-turbulence intensity profile at $R=0.721$.

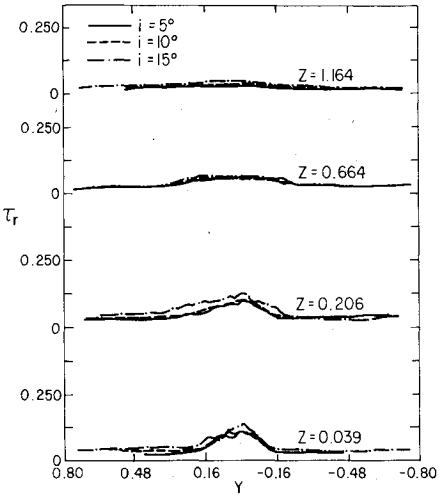

Fig. 4 Radial-turbulence intensity profile at $R=0.721$.

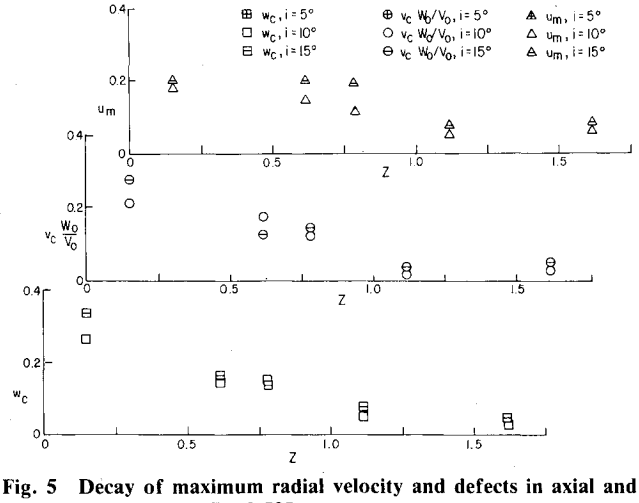

Fig. 5 Decay of maximum radial velocity and defects in axial and tangential velocities at $R=0.535$.

tangential velocity defects in the wake are found to have decayed slower at $R=0.535$ and 0.907, 20% of the span from the hub and end walls, respectively, than at midradius ($R=0.721$). Larger radial velocities were also measured in the rotor wake for the stations away from midspan. This indicates a larger radial migration of mass and momentum in the wake at $R=0.535$ and 0.907 than at $R=0.721$. The above spanwise wake characteristics may result from the effects of the hub- and end-wall boundary layers on the wake or secondary flow effects.

When studying the rate of decay of velocity defects it should be noted that for a given Z position, larger s/c locations are found for increasing radius since the rotor wake decays along relative streamlines.

Radial Variation of Wake Centerline Velocity or Defect

Spanwise variations of axial and tangential mean velocity defects and maximum radial mean velocity difference in the far wake are shown in Figs. 8, 9, and 10, respectively. Data are shown in the far wake for measurement stations at Z (midspan) = 1.664 (station 1), 1.164 (station 4), and 0.831 (station 6) for rotor blade incidences of 10 and 15 deg.

Axial mean velocity defect variation with radius is shown in Fig. 8. Data at station 6 for both rotor blade incidences (10 and 15 deg) show a decrease in axial velocity defect for increasing radius except between $R=0.628$ and 0.721, where the defect is approximately constant. This trend is as expected with streamwise distance downstream of the rotor in the relative frame of reference increasing for increasing radius. However, axial mean velocity defect is significantly larger for $R=0.535$ than for other radial locations for station 6. This may result from the effects of the hub-wall boundary layer on the wake decay characteristics.

The axial velocity defects for stations 1 and 4 in Fig. 8 show relatively small changes for varying radius. Measurements made at these stations are sufficiently far downstream so that the axial velocity defect is small for all radial locations. The data shown for stations 1 and 4 do show slightly larger axial velocity defects towards the hub- and end-wall boundary layers. Axial defect for $R>0.721$ would be expected to decrease for increasing radius since streamwise distance from the rotor is larger. This increase in axial velocity defect indicates the effects of radial transport of mass and momentum and end-wall flows on the rotor wake.

The effect of increasing rotor blade incidence on axial velocity defect is small for the far-wake measurement stations shown in Fig. 8. Axial velocity defect is found to be slightly larger for the 15-deg operating condition than for the 10-deg operating condition for almost all of the data shown.

Variation of tangential velocity defect with radius, shown in Fig. 9, clearly indicates the three-dimensional effects on the rotor-wake flow. For the measurements at 10 deg incidence shown for all stations, the tangential velocity defect is found to increase with radius for $R>0.721$. For the 15-deg operating condition, the tangential velocity defect increases for $R>0.628$. At both 10 and 15 deg rotor blade incidences at station 6 the defect also increases towards the hub wall as indicated by the data at $R=0.535$. Defect in tangential velocity is expected to decrease for increasing radius with larger s/c locations found at larger radial positions. Secondary flows near the hub wall may account for the increase in tangential velocity defect in this region. Strong end-wall flow effects, either tip vortex or secondary flows, result in the increased tangential velocity defects found for increasing radius beyond midspan. The radial transport of mass and momentum may also account for the increased tangential velocity defects. The effects of the hub- and end-wall flows are shown to be weaker at these stations since they are farther downstream from the rotor.

The effects of varying blade loading on the tangential velocity defect are clearly shown in Fig. 9. Tangential velocity defect is found to increase for increased blade loading except

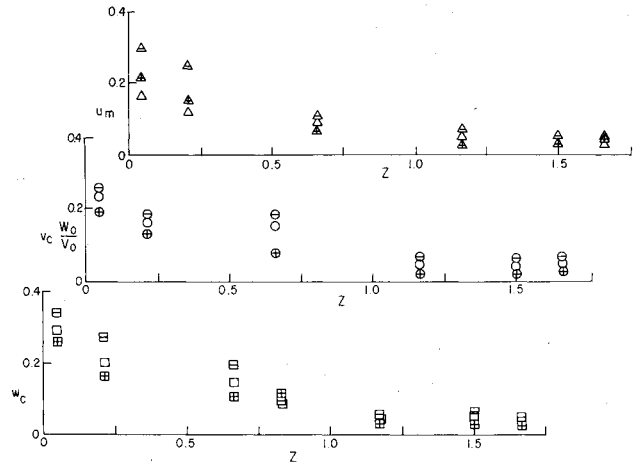

Fig. 6 Decay of maximum radial velocity and defects in axial and tangential velocities at $R=0.721$; legend defined in Fig. 5.

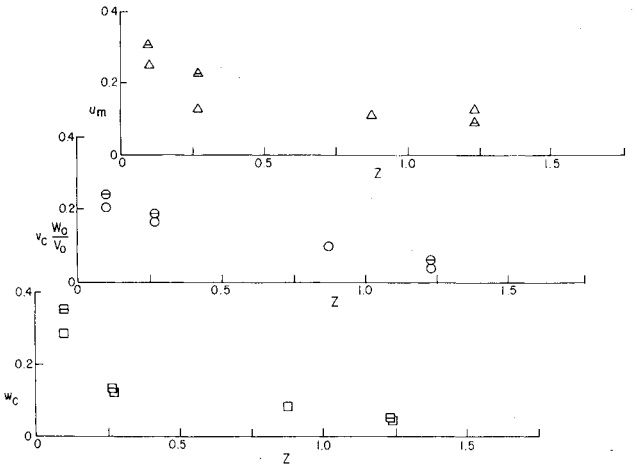

Fig. 7 Decay of maximum radial velocity and defects in axial and tangential velocities at $R=0.907$; legend defined in Fig. 5.

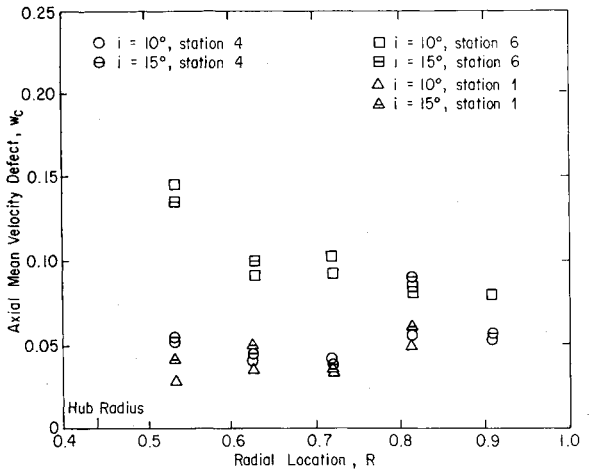

Fig. 8 Radial variation of axial velocity defect at the wake centerline.

for some scatter in the data at station 6 for $R=0.535$. The increase in tangential velocity defects in Fig. 9 are slightly more pronounced than the corresponding axial velocity defects shown in Fig. 8. This is consistent with the rotor-wake characteristics results reported in Ref. 1 at midradius.

The effects of varying radius on the maximum radial velocity differences in the rotor wake at stations 1 and 4 are shown in Fig. 10. Radial velocities in the wake are seen to be

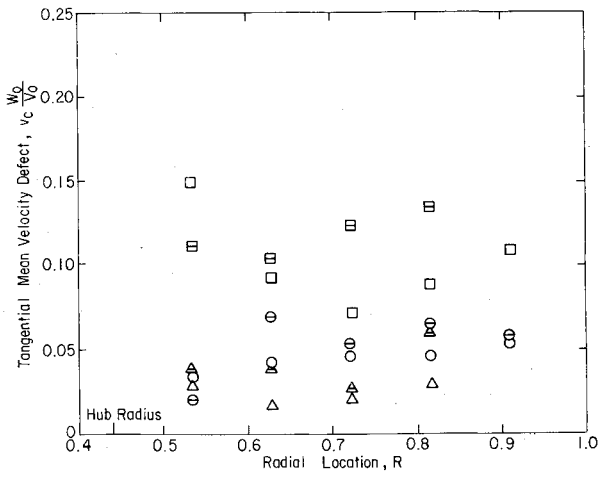

Fig. 9 Radial variation of tangential velocity defect at the wake centerline; legend defined in Fig. 8.

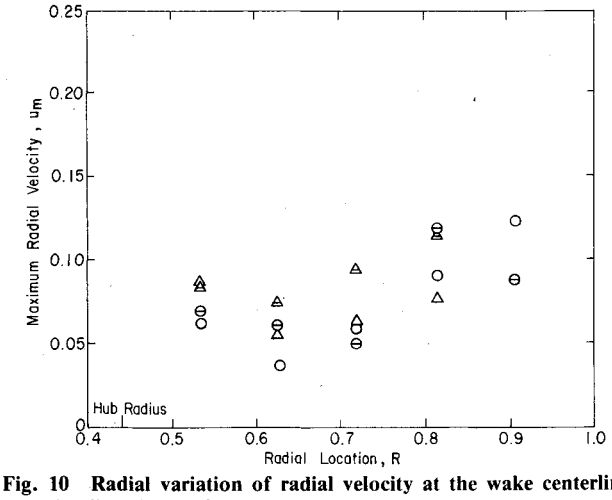

Fig. 10 Radial variation of radial velocity at the wake centerline; legend defined in Fig. 8.

significant at rotor blade incidences of 10 and 15 deg for both of the far-wake stations. This indicates that the rotor wake is highly three-dimensional with a large radial transport of mass, momentum, and energy in the far-wake region. This radial transport will result in small defects in axial and tangential mean velocities as shown in Figs. 8 and 9, respectively. An increase in radial velocity difference in the wake is clearly shown for increasing radius past midspan. This increase in radial velocities across the wake shows the effects of strong radial pressure gradients and end-wall flows. The increase of maximum radial velocity difference towards the hub may indicate the effects of secondary flows near the hub wall.

Decay of Maximum Turbulence Intensities Downstream

The decay of maximum axial-, tangential-, and radial-turbulence intensities in the rotor wake are shown for $R=0.535$ and 0.721 in Figs. 11 and 12, respectively. Wake measurements are shown for the rotor operating at blade incidences of 5, 10, and 15 deg.

For all of the spanwise measurement stations the effects of varying blade loading are clearly seen. Increased rotor blade incidence resulted in increased axial-, tangential-, and radial-turbulence intensity levels. This wake characteristic is still evident in the far downstream region for $Z>1.0$. At $R=0.535$ the effects of increased blade loading are found to be more pronounced (in the near-wake region) than at $R=0.721$ and 0.907. The turbulent nature of the wake was found to behave differently with varying blade loading than the mean velocity components which did not exhibit this spanwise variation.

A slow decay of axial-, tangential-, and radial-components of turbulence intensity is found in the near- and far-wake regions for all three spanwise positions. Turbulence intensity characteristics in the far wake are influenced by adjacent blade wakes, accounting for the asymptotic decay behavior measured in this region. The near- and far-wake decay rates are not shown to be significantly altered by the spanwise position.

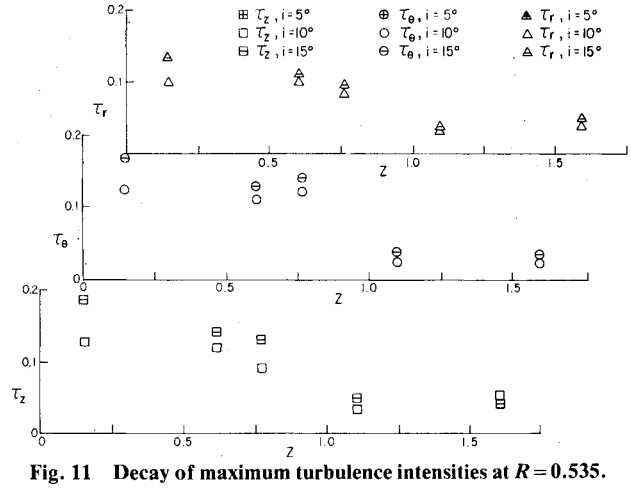

Fig. 11 Decay of maximum turbulence intensities at $R=0.535$.

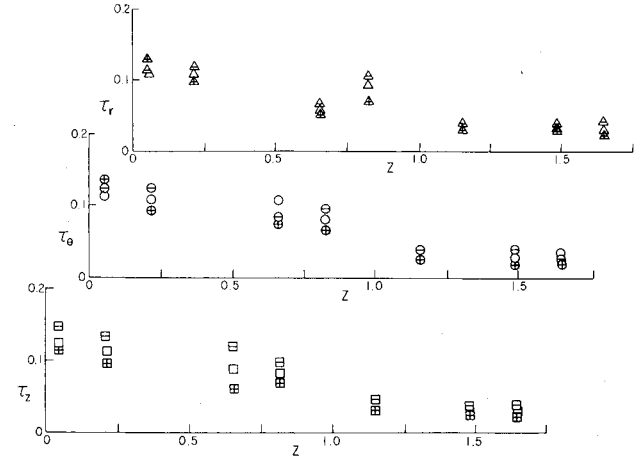

Fig. 12 Decay of maximum turbulence intensities at $R=0.721$; legend defined in Fig. 11.

Radial Variation of Maximum Turbulent Intensities

The radial variation of maximum axial-, tangential, and radial-turbulence intensities in the far wake is shown in Figs. 13, 14, and 15, respectively. Measurements are shown for rotor blade incidences of 10 and 15 deg at stations 1, 2, and 4 ($Z=1.664$, 1.498, and 1.164 at midradius, respectively). At all the stations, the maximum axial-, tangential-, and radial-turbulence intensities in the wake show the lowest values near midradius at $R=0.628$ and 0.721. All components of maximum intensities show similar increases toward the hub- and end-wall radii. This trend is still very pronounced at the farthest downstream station (station 1). The hub- and end-wall flows are therefore found to alter, substantially, the axial-, tangential, and radial-turbulence intensities in the rotor wake. Hence the resulting periodic and unsteady inlet conditions to a subsequent blade row due to the rotor wake would not be radially uniform for turbulence intensities. It is shown to be uniform near midradius for approximately 20% of the radius.

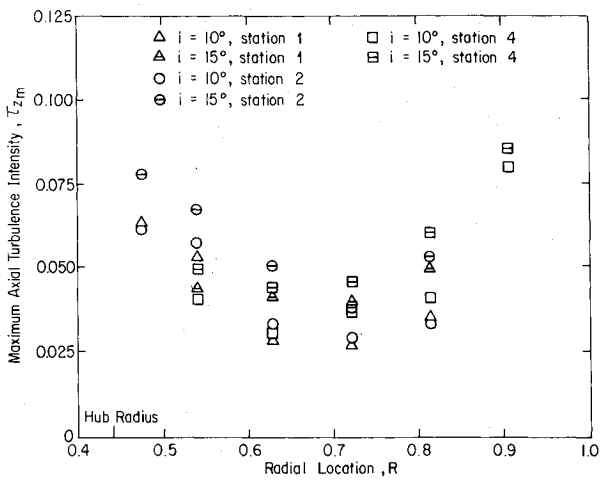

Fig. 13 Radial variation of maximum axial-turbulence intensity.

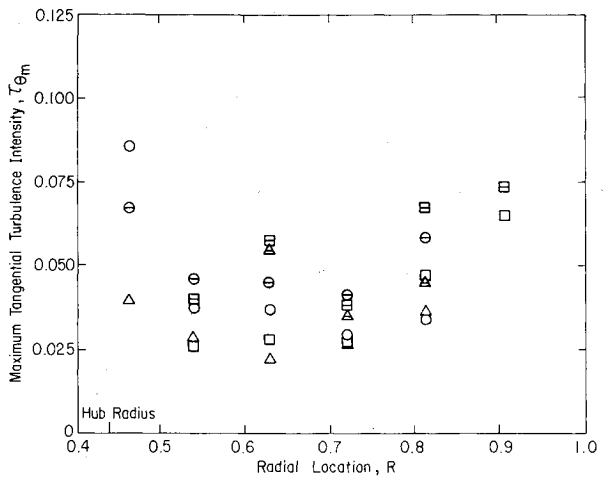

Fig. 14 Radial variation of maximum tangential-turbulence intensity; legend defined in Fig. 13.

The presence of maximum radial intensities of the same order of magnitude as the axial and tangential components in the rotor wake indicates the three-dimensional structure of the turbulence. This characteristic is present at all radial locations for both rotor blade incidences (10 and 15 deg) even for measurements far downstream at station 1.

Wake Width and Momentum Thickness

The variation of semiwake width with radius is shown in Fig. 16 for measurements made at stations 1 and 4 with rotor blade incidences of 10 and 15 deg. For all measurements shown in Fig. 16, the lowest value of wake width is at midradius ($R = 0.721$). A large increase in wake width is found for increasing radius beyond midradius. This represents the effects of the large radially outward transport of mass, momentum, and energy in the rotor wake. A smaller increase in semiwake width near the hub wall is also shown in Fig. 16. This characteristic may result from the hub-wall boundary layer and secondary flow effects on the rotor wake.

The wake momentum thickness variation downstream of the rotor is shown in Fig. 17. Rotor-wake data for the 5-, 10-, and 15-deg operating conditions are shown for measurements made at midradius ($R = 0.721$) in both the near- and far-wake regions. Also shown in Fig. 17 are isolated airfoil data due to Preston et al.[3] and cascade data from Raj and Lakshminarayana.[4]

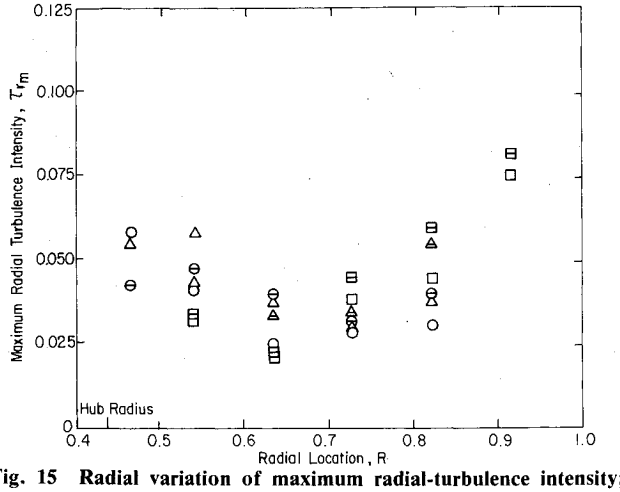

Fig. 15 Radial variation of maximum radial-turbulence intensity; legend defined in Fig. 13.

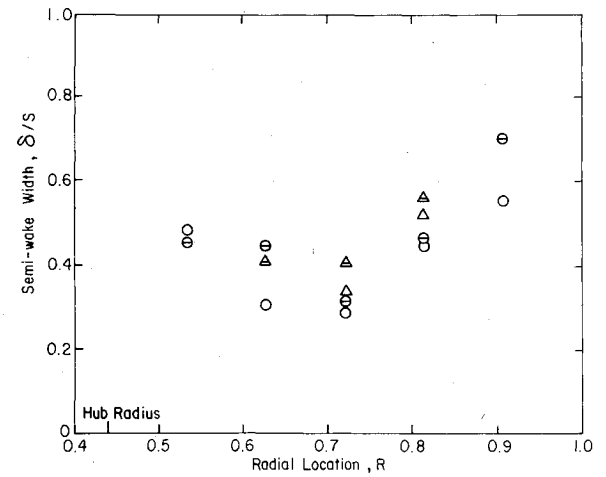

Fig. 16 Radial variation of semiwake width; legend defined in Fig. 8.

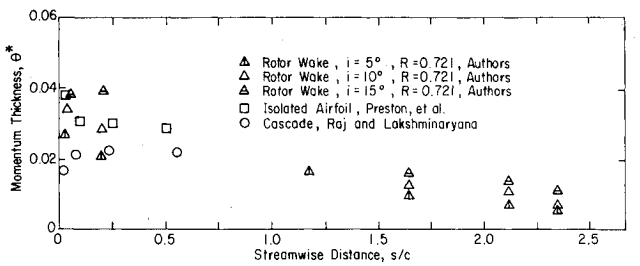

Fig. 17 Streamwise variation of momentum thickness for airfoil, cascade and rotor wakes.

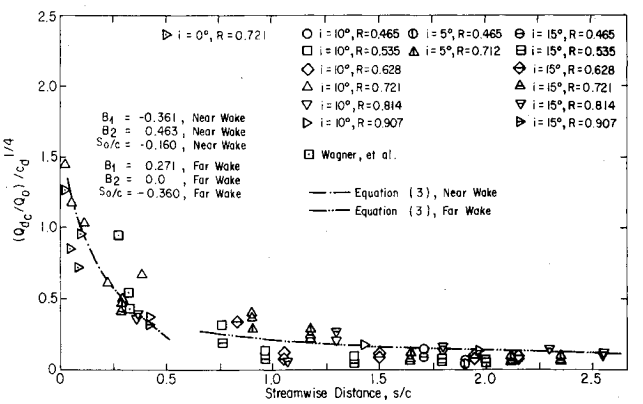

Fig. 18 Rotor wake correlation for the total velocity defect with $(C_D)^{1/4}$.

Momentum thickness for the rotor wake was determined using the equation

$$\theta^* = \frac{1}{S}\int_o^S \frac{Q}{Q_o}\left(1-\frac{Q}{Q_o}\right)rd\theta$$

where integration was performed in the tangential direction across one blade spacing. The variations of momentum thickness for the flat plate, isolated airfoil, cascade, and rotor wakes are shown in Fig. 17. The momentum thickness for the isolated airfoil and cascade wake are shown to decrease and increase, respectively, in the near-wake region and then to approach nearly constant values in the far wake. These trends are explained by Raj and Lakshminarayana.[4]

The momentum thickness for the rotor wake at midradius for 5 and 10 deg incidences is shown to decrease initially and then to approach nearly constant values at the far downstream stations. At $i=15$ deg, the momentum thickness is found to increase slightly in the near wake and then to decrease to a nearly constant value at the far downstream locations. For all of the rotor-wake measurements at midradius, increased blade loading is shown to result in larger momentum thicknesses. This indicates that a larger momentum deficit exists in the rotor wake for increased blade loading. A larger momentum deficit may result from an increased radial transport of momentum. Reynolds[2] has provided a theoretical explanation for this behavior.

Rotor-Wake Correlation

Correlation of the far-wake data behind a body was determined theoretically by Schlichting[5] using the drag coefficient C_D to collapse the mean velocity data from different configurations into a single curve. The analysis of the two-dimensional turbulent far wake given in Ref. 5 indicates a dependency of the type

$$Q_{d_c}/Q_o = C_D^{1/2} f_1(s/c) \tag{1}$$

However, Silverstein et al.,[6] and Silverstein and Katzoff[7] show a good correlation for measurements made behind an isolated airfoil using a different functional dependence for C_D than that given in Eq. (1). This functional dependence was given as

$$Q_{d_c}/Q_o = C_D^{1/4} f_2(s/c) \tag{2}$$

Correlated wake defect data were examined using the relationships given by Eqs. (1) and (2). The correlation based on Eq. (2), shown in Fig. 18, provided better agreement with the data in the near wake (except for the trailing-edge region) and similar agreement with data in the far-wake region than that from Eq. (1). Hence the correlation given by Eq. (2) has been used in providing an expression for the wake decay characteristics, which include the loading and spanwise effects, through the drag coefficient parameter.

The rotor-wake correlation is shown in Fig. 18, using data from the present investigation and from Wagner et al.[8] The correlated data show reasonable agreement with the equation

$$\frac{Q_{d_c}}{Q_o} = C_D^{1/4}\left[B_1\left(\frac{s}{c}-\frac{s_o}{c}\right)^{-1/2} + B_2\left(\frac{s}{c}-\frac{s_o}{c}\right)^{-1}\right] \tag{3}$$

in both the near- and far-wake regions. The functional dependence with s/c is shown in the far-wake region for $B_2=0.0$. Constants B_1 and B_2 and virtual origins s_o for each curve are given in Fig. 18.

Conclusions

The major conclusions derived on the basis of the measurements presented and discussed in this paper follow:

1) The rotor-wake mean velocity profiles are found to be highly asymmetric about the wake centerline. This characteristic is more pronounced for increased blade loadings at all spanwise positions.

2) The decay rates for axial, tangential, and radial mean velocities and turbulence intensities were nearly the same at all spanwise positions. This characteristic was evident in both the near- and far-wake regions.

3) Large radial mean velocities in the rotor wake in the near-wake region indicate a large radial migration of mass, momentum, and energy at all spanwise measurement stations.

4) The rotor-wake width is found to significantly increase at spanwise positions away from midradius, particularly towards the end wall region. The large wake thickness measured above midradius may result from the large radial transport of mass, momentum, and energy in the rotor wake.

5) Momentum thickness is shown to decrease with increasing axial distance in the near-wake region, and reaches an almost constant value in the far-wake region.

6) All components of mean velocity defect and turbulence intensity increased for larger blade loading at all spanwise measurement stations. These characteristics were discernible in both the near- and far-wake regions.

7) The resultant relative velocity defect in the rotor wake showed a good correlation with $C_D^{1/4}$ at all spanwise positions in the near- and far-wake regions.

Acknowledgments

This work was supported by the National Aeronautics and Space Administration through Grant NSG 3012 with L. Shaw as the technical monitor. Assistance by A. Ravindranath in acquiring the wake data is gratefully acknowledged. The experimental work was carried out at the Applied Research Laboratory in their Axial Flow Research fan facility. Assistance by J. Rishell and W. Nuss in gratefully acknowledged.

References

[1] Reynolds, B., Lakshminarayana, B., and Ravindranath, A., "Characteristics of the Near Wake of a Compressor or a Fan Rotor Blade," *AIAA Journal,* Vol. 17, Sept. 1979, pp. 959-967.

[2] Reynolds, B. and Lakshminarayana, B., "Characteristics of Lightly Loaded Fan Rotor Blade Wake," NASA CR 3188, Oct. 1979.

[3] Preston, J.H. and Sweeting, N.E., "The Experimental Determination of the Boundary Layer and Wake Characteristics of Simple Joukowski Airfoils with Particular Reference to the Trailing Edge Region," British ARC R&M 1998, 1943.

[4] Raj, R. and Lakshminarayana, B., "Characteristics of the Wake Behind a Cascade of Airfoils," *Journal of Fluid Mechanics,* Vol. 61, 1973, pp. 707-730.

[5] Schlichting, H., *Boundary Layer Theory,* McGraw-Hill, Inc., New York, 1968, pp. 685-686.

[6] Silverstein, A., Katzoff, S., and Bullivant, W.K., "Downwash and Wake Behind Plain Airfoils," NACA Rept. 651, 1939.

[7] Silverstein, A. and Katzoff, S., "Design Charts for Predicting Downwash Angles and Wake Characteristics Behind Plain and Flapped Wings," NACA Rept. 648, 1939.

[8] Wagner, J.H., Okiishi, T.H., and Holbrook, G.J., "Periodically Unsteady Flow in an Imbedded Stage of a Multistage, Axial-Flow Turbomachine," *Journal of Engineering for Power,* Vol. 101A, 1979, pp. 42-51.